ACS EARTH AND SPACE CHEMISTRY

http://pubs.acs.org/journal/aesccq

Article

# Large Variations in Hygroscopic Properties of Unconventional Mineral Dust

Chao Peng,◆ Wenjun Gu,◆ Rui Li, Qinhao Lin, Qingxin Ma, Shiguo Jia, Padmaja Krishnan, Xinming Wang, and Mingjin Tang*

Cite This: *ACS Earth Space Chem.* 2020, 4, 1823−1830

Read Online

ACCESS | Metrics & More | Article Recommendations | Supporting Information

**ABSTRACT:** Unconventional mineral dust, such as fly ash, road dust, and industrial dust, could significantly contribute to fine particulate matters; however, their hygroscopicity remains largely unexplored. In this work, a vapor sorption analyzer and a diffusion reflectance infrared Fourier transform spectroscopy (DRIFTS) were used to examine hygroscopic properties of 11 unconventional mineral dust samples as a function of relative humidity (RH) at 25 °C, including two municipal waste fly ash, one oil fly ash, one road dust, and seven coal fly ash. Large variations in hygroscopicity were observed for the 11 samples, and mass ratios of adsorbed water to the dry samples at 90% RH were found to vary from 0.0003 to 0.7340, showing positive dependence on both water-soluble ion contents and BET surface areas. In addition, hygroscopicity of the 11 unconventional mineral dust samples examined could be well described by the Freundlich adsorption isotherm model, with $A_F$ and $B_F$ parameters found to be in the range of $3.5 \times 10^{-4}$−1.29 and 0.12−1.58, respectively. Our study would significantly improve our knowledge of hygroscopicity properties of unconventional mineral dust.

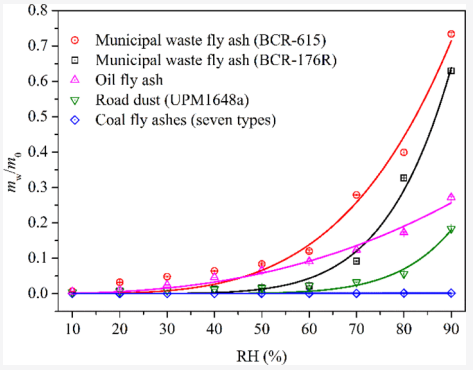


**KEYWORDS:** *unconventional mineral dust, fly ash, hygroscopicity, water adsorption, water-soluble content*



## INTRODUCTION

Mineral dust is an important type of aerosol in the troposphere, with an annual global flux of ∼2000 Tg yr.$^{-1}$.[1,2] It is conventionally believed that mineral dust has two major sources, i.e., natural and anthropogenic windblown dust.[3] However, recent studies have suggested that other sources related to human activities, such as coal combustion and industrial processes, could contribute to mineral dust in urban areas and have been called anthropogenic fugitive, combustion, and industrial dust (AFCID);[4−9] hereinafter referred to as unconventional mineral dust in our study.

With rapid urbanization and industrialization across the globe, the emission of unconventional mineral dust may increase in the future; however, its global fluxes and mass loadings have not been widely considered in regional and global models yet.[10−13] Philip et al.[12] estimated an increase of 2−16 $\mu$g m$^{-3}$ (∼10%) in $PM_{2.5}$ over the globe after considering unconventional mineral dust emissions. A very recent study[14] revealed that up to 45 $\mu$g m$^{-3}$ for $PM_{10}$ in eastern China during winter could be contributed by unconventional mineral dust. Furthermore, Chen et al.[9] suggested that unconventional mineral dust, such as road dust, is a major source of urban $PM_{2.5}$, accounting for 16−52% of the urban $PM_{2.5}$ emission.

Fly ash, a byproduct of combustion, is one of the most abundant unconventional mineral dust with an estimated annual emission of ∼300 Tg yr.$^{-1}$ across the globe.[15] A number of studies suggested that fly ash could participate in atmospheric processes and affect the atmospheric environment, climate, and the hydrological cycle.[16−22] For example, fly ash has been found to be an important source of iron, and therefore, it may contribute to the sulfate formation and global sulfur cycle via the transition metal ion catalysis pathway.[17,23,24] Moreover, as a source of bioavailable iron, fly ash particles can deposit into open oceans through long-distance transport processes, thus affecting the biogeochemical cycle and carbon uptake, and enhancing the oceanic primary productivity.[18,25−27] Fly ash particles can also affect the Earth's radiative budget and climate by acting as cloud condensation nuclei (CCN) or ice nuclei (IN) in the troposphere.[19,21,28−31] In addition, it is suggested that fly ash particles have a negative impact on human health, such as increasing the susceptibility of the airways to bacterial infection and the risk of mortality and respiratory diseases.[32,33]

**Received:** August 13, 2020
**Revised:** September 13, 2020
**Accepted:** September 26, 2020
**Published:** September 26, 2020

Table 1. Water-Soluble Inorganic Ion Contents (mg/g) and the BET Surface Areas ($m^2/g$) for the 11 Samples Investigated in this work[a]

| sample | $Na^+$ | $NH_4^+$ | $K^+$ | $Ca^{2+}$ | $Mg^{2+}$ | |
|---|---|---|---|---|---|---|
| BCR-176R | 27.13 ± 0.46 | n.d. | 28.36 ± 0.47 | 0.04 ± 0.01 | 72.07 ± 1.11 | |
| BCR-615 | 21.43 ± 1.40 | 0.37 ± 0.03 | 14.01 ± 0.90 | 0.17 ± 0.08 | 74.23 ± 4.73 | |
| OFA | 43.42 ± 0.66 | n.d. | 5.10 ± 0.21 | 24.83 ± 2.65 | 2.55 ± 0.24 | |
| UPM1648a | 39.18 ± 0.88 | 12.05 ± 0.36 | 7.16 ± 0.03 | 57.28 ± 8.52 | 7.09 ± 0.56 | |
| CFA-2689 | 0.09 ± 0.01 | n.d. | n.d. | n.d. | 8.78 ± 0.56 | |
| CFA-2690 | 0.11 ± 0.01 | n.d. | n.d. | 0.41 ± 0.03 | 6.40 ± 0.20 | |
| CFA-2691 | 0.47 ± 0.01 | n.d. | n.d. | 1.51 ± 0.09 | 73.15 ± 1.44 | |
| GBW08401 | n.d. | n.d. | n.d. | 0.16 ± 0.02 | 9.67 ± 0.66 | |
| GBW11128a | n.d. | n.d. | n.d. | n.d. | 24.37 ± 0.24 | |
| GBW11129a | n.d. | n.d. | n.d. | n.d. | 6.51 ± 0.65 | |
| GBW11131a | n.d. | n.d. | n.d. | n.d. | 4.02 ± 0.03 | |
| sample | $F^-$ | $Cl^-$ | $NO_3^-$ | $SO_4^{2-}$ | total | BET |
| BCR-176R | 1.24 ± 0.33 | 67.90 ± 1.81 | n.d. | 82.79 ± 2.53 | 279.53 ± 5.40 | 3.02 ± 0.05 |
| BCR-615 | 0.52 ± 0.06 | 76.18 ± 4.58 | n.d. | 93.02 ± 5.28 | 279.92 ± 16.94 | 1.79 ± 0.03 |
| OFA | n.d. | 25.62 ± 1.08 | 25.42 ± 5.11 | 117.23 ± 24.51 | 244.17 ± 34.46 | - |
| UPM1648a | n.d. | 30.61 ± 5.39 | 30.59 ± 0.16 | 136.23 ± 10.36 | 320.19 ± 26.26 | 3.15 ± 0.03 |
| CFA-2689 | n.d. | n.d. | n.d. | 6.85 ± 0.32 | 15.72 ± 0.83 | 0.40 ± 0.02 |
| CFA-2690 | n.d. | n.d. | n.d. | 3.13 ± 0.09 | 10.06 ± 0.32 | 1.44 ± 0.05 |
| CFA-2691 | n.d. | n.d. | n.d. | 15.98 ± 0.23 | 91.12 ± 1.33 | 0.63 ± 0.02 |
| GBW08401 | n.d. | n.d. | n.d. | 3.39 ± 0.08 | 13.22 ± 0.75 | 1.59 ± 0.04 |
| GBW11128a | n.d. | n.d. | n.d. | 40.91 ± 0.99 | 65.28 ± 0.74 | 1.61 ± 0.02 |
| GBW11129a | n.d. | n.d. | n.d. | 3.35 ± 0.57 | 9.86 ± 1.22 | 0.58 ± 0.01 |
| GBW11131a | n.d. | n.d. | n.d. | 3.55 ± 0.23 | 7.57 ± 0.23 | 0.53 ± 0.01 |

[a]Note: n.d. = not detected; BET surface area of OFA was not obtained due to continuous evaporation of its volatile residues at the degassing temperature (413 K).

Hygroscopic properties determine the liquid water content of aerosol particles under ambient conditions,[34] thereby affecting their optical properties, heterogeneous reactivity, and dry and wet deposition. As reviewed by Tang et al.,[35] a number of studies investigated hygroscopic properties of conventional mineral dust; in general, the hygroscopicity of conventional mineral dust was found to be quite low, with single hygroscopicity parameters ($\kappa$) < 0.01.[35] However, to our knowledge, only one previous study has investigated the water uptake properties of unconventional mineral dust.[36] Navea et al.[36] studied the water adsorption on four kinds of fly ash samples using a quartz crystal microbalance (QCM) coupled with an attenuated total reflection Fourier transform infrared (ATR-FTIR) spectroscopy, demonstrating that the water uptake behaviors of different fly ashes were indeed different. Specifically, it was found that the mass ratios of adsorbed water to dry samples ($m_w/m_0$) at 60% relative humidity (RH) varied from 2.23 to 15.34% for different fly ash. As a result, one can conclude that hygroscopic properties of unconventional mineral dust (including fly ash) have not been well understood, especially at high RH.

In this work, two complementary techniques were used to investigate water uptake properties of 11 unconventional mineral dust, including seven coal fly ash, two municipal waste fly ash, one oil fly ash, and one road dust. A vapor sorption analyzer (VSA) and an in situ diffusion reflectance infrared Fourier transform spectroscopy (DRIFTS) were employed to measure the amounts of water adsorbed on these samples as a function of RH at room temperature.

## EXPERIMENTAL SECTION

**Sample Characterization.** The oil fly ash (OFA) was collected from a heavy oil-fired boiler,[37] and the remaining samples were reference materials obtained commercially. Two European municipal waste fly ash, including incineration ash (BCR-176R) and fly ash (low level) (BCR-615), were obtained from the European Commission Community Bureau of Reference; three American coal fly ash (CFA-2689, CFA-2690 and CFA-2691) were procured from the National Institute of Standards and Technology. Among the four Chinese coal fly ash, the GBW08401 sample was obtained from the Research Center for Eco-Environmental Sciences, Chinese Academy of Sciences, while GBW11128a, GBW11129a, and GBW11131a samples were obtained from the Test Center of China Coal Research Institute. The road dust sample (UPM1648a) was provided by the National Institute of Standards and Technology. All the samples were used without further pretreatment.

Water-soluble inorganic ion contents were measured using ion chromatography (Metrohm 761 Compact IC, Metrohm, Herisau, Switzerland), and details can be found in our previous work.[38,39] The mass concentrations of five cations ($Na^+$, $NH_4^+$, $K^+$, $Ca^{2+}$, and $Mg^{2+}$) and six anions ($F^-$, $Cl^-$, $Br^-$, $NO_2^-$, $NO_3^-$, and $SO_4^{2-}$) in the solutions were quantified with the detection limits being ~0.02 mg/L.

An accelerated surface area and porosimetry analyzer (ASAP 2020 PLUS, Micromeritics, Georgia, USA) was employed to determine the Brunauer–Emmett–Teller (BET) surface areas. The BET surface area of OFA could not be measured due to the continuous evaporation of its volatile residues at the degassing temperature (413 K). Further information related to the BET analysis can be found elsewhere.[40]

**Hygroscopicity Measurements.** Water adsorption on unconventional mineral dust samples was investigated using two experimental approaches. An in situ DRIFTS was used to detect the change of infrared spectra of sample particles in the


https://dx.doi.org/10.1021/acsearthspacechem.0c00219
ACS Earth Space Chem. 2020, 4, 1823–1830

range of 0−90% RH. Measurement procedures were detailed in previous studies,[41,42] and thus, only a brief description is provided here. Infrared spectra of samples were recorded as a function of RH at 25 °C, using a Fourier transformation infrared spectrometer (Nicolet 6700, Thermo Nicolet Instrument Corporation), equipped with an in situ diffuse reflection chamber and a high-sensitivity mercury cadmium telluride (MCT) detector cooled by liquid $N_2$. The RH (0−90%) in the chamber was controlled by adjusting the mixing ratio of dry and humidified $N_2$ flows, with an uncertainty of ±2% RH. The total gas flow was set to 200 mL $min^{-1}$, and the sample mass for each measurement was typically around 10 mg. All the spectra reported in this work were recorded at 4 $cm^{-1}$ resolution by averaging 100 scans.

A vapor sorption analyzer (Q5000SA, TA instruments, Delaware, USA) was used to measure the mass change of samples as a function of RH (0−90%) at 25 °C. Experimental details have been provided in our previous studies.[42−45] Briefly, a high-precision balance was employed to measure the sample mass change at different RHs, with an absolute uncertainty of <0.1 μg. In a typical experiment, the sample was first dried at <1% RH; then, the RH was stepwise increased to 90% with an interval of 10%; finally, the sample was dried at <1% RH again. RH would not be changed to the next value until the mass change of the sample was <0.05% in 30 min, when the sample was considered to reach an equilibrium with water vapor. In some experiments, we changed RH only after the change in sample mass was <0.05% in 60 min (instead of 30 min for most experiments), and no difference in measured mass growth was observed between the two experimental conditions. The dry mass of each sample used was usually around 1.0 mg. For each sample examined in this work, at least three measurements were conducted, and the average mass changes and standard deviations are reported.

## RESULTS AND DISCUSSION

**Sample Characterization.** The water-soluble inorganic ion contents (mg/g) of all the 11 samples studied in this work are summarized in Table 1. For cations, $Mg^{2+}$ was detected in all the samples (2.55−74.23 mg/g), and the mass fractions of $Na^+$, $K^+$, and $Ca^{2+}$ were found to vary among the different samples by four orders of magnitude; in addition, $NH_4^+$ was only detected in two samples (BCR-615 and UPM1648a). For anions, $SO_4^{2-}$ was the major component for all the samples (3.13−136.23 mg/g), and samples other than coal fly ash were also found to contain $Cl^-$ (25.62−76.18 mg/g); nevertheless, $NO_3^-$ was only detected in UPM1648a and OFA samples, and $Br^-$ and $NO_2^-$ were always below the detection limits. The total mass fractions of water-soluble inorganic ions showed larger variations (7.57−320.19 mg/g) for the 11 samples examined. Their BET surface areas were found to range from 0.40 ± 0.02 $m^2/g$ (CFA-2689) to 3.15 ± 0.03 $m^2/g$ (UPM1648a), as summarized in Table 1.

**Hygroscopic Properties.** *DRIFTS Spectra of Samples at Different RHs.* Figure 1 shows typical DRIFTS spectra for BCR-176R at different RHs. The spectra for the other samples can be found in Figures S1 and S2. As shown in Figure 1, several IR peaks (3593, 3468, 3401, 3322, 1659, and 1628 $cm^{-1}$) appeared with the increase in RH (spectrum at <1% RH was used as the baseline), and their intensities increased with RH. Similar observations were also reported by Navea et al.[36] As suggested in previous studies,[35,36,41,46−49] these peaks can be attributed to the adsorbed water. The broad band in the

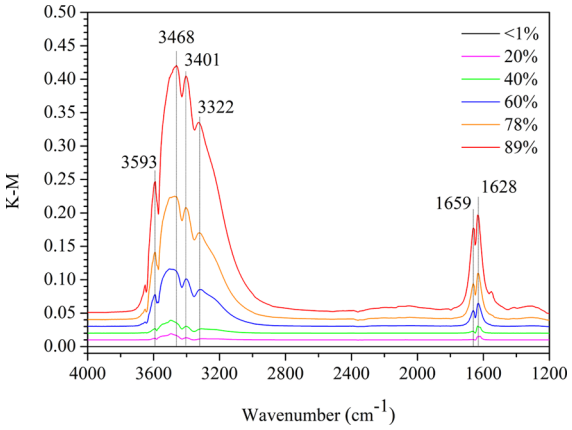


**Figure 1.** In situ DRIFTS spectra of BCR-176R (incineration ash) as a function of RH (<1, 20, 40, 60, 78, and 89%) at 25 °C.

range of 3000−3800 $cm^{-1}$ is assigned to O−H stretching vibrational modes, including symmetric and asymmetric stretching, and the two peaks at ∼1628 and ∼1659 $cm^{-1}$ are assigned to the bending mode of liquid water and microporous amorphous ice, respectively.[47] The broad peak in the range of 3000−3800 $cm^{-1}$ was the most intense in the entire spectrum, and thus the integrated areas of this characteristic peak were calculated to represent the amount of water adsorbed at different RHs. The results are summarized in Table S1, showing that the amount of adsorbed water increased with RH.

*Mass Hygroscopicity Growth.* In order to precisely quantify the mass change of adsorbed water at different RHs, mass growth factors of unconventional mineral dust samples were measured using a VSA. Figure 2 displays RH and normalized sample mass (normalized to that at <1% RH) changes with time for two typical measurement experiments. For example, the normalized mass of BCR-176R increased with RH, reaching 1.09, 1.33, and 1.63 at 70, 80, and 90% RH, respectively. The mass ratios of adsorbed water to the dry sample ($m_w/m_0$) as a function of RH for all samples are summarized in Table S2.

To our knowledge, water adsorption on BCR-176R was investigated by Navea et al.[36] using a quartz crystal microbalance (QCM) in the range of 0−61% RH at room temperature. As shown in Figure 3, Navea et al.[36] suggested that the sample mass was increased by 5.3, 9.2, and 15.3% at 20, 40, and 60% RH, significantly higher than our results (0.7, 1.3, and 2.2% at 20, 40, and 60% RH). One reason is that the underlying assumptions required to convert the QCM signals to the relative change in sample mass may not always be fulfilled, as discussed in a recent review paper.[34] However, when extrapolating to higher RH, the mass increase would be 32.4% at 80% RH and 66.2% at 90% RH, consistent with our study (i.e., 32.7% at 80% RH and 63.0% at 90% RH, respectively). Due to rare experimental reports about the water adsorption on unconventional mineral dust, further investigations using similar or different techniques[34] are highly warranted and would be very valuable.

Several theories and models have been used to quantitatively describe water adsorption and hygroscopic growth under subsaturated conditions.[35] As shown in Figure 4 and Figure S3, we found that the Freundlich adsorption isotherm model could fit our experimental data well, and $R^2$ was found to be >0.88 for all the samples. The Freundlich adsorption isotherm model can be expressed by the following equation:[35,50]


https://dx.doi.org/10.1021/acsearthspacechem.0c00219
ACS Earth Space Chem. 2020, 4, 1823−1830

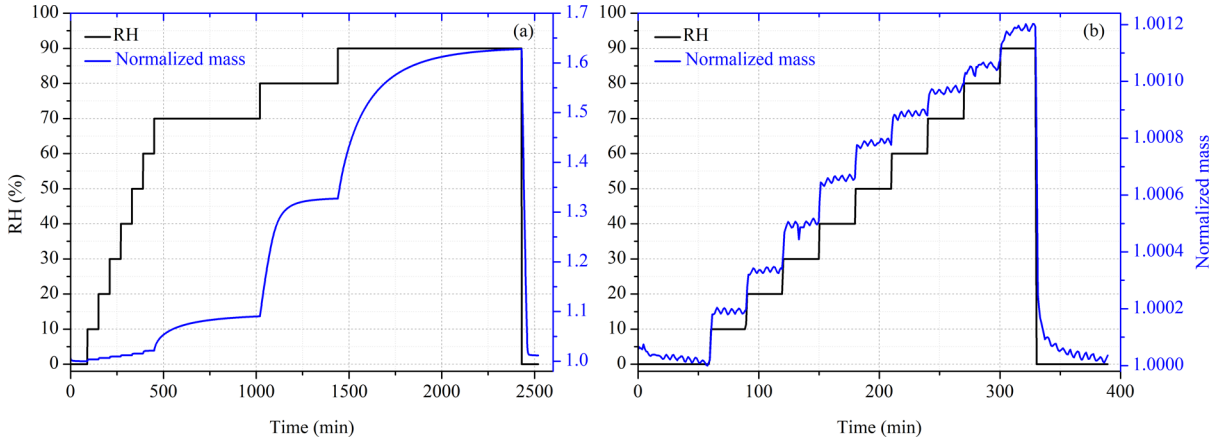


**Figure 2.** RH (black curve, left *y* axis) and normalized sample mass (blue curve, right *y* axis) as a function of time in two typical mass hygroscopic growth measurement experiments at 25 °C: (a) BCR-176R (incineration ash) and (b) CFA-2690 (coal fly ash).

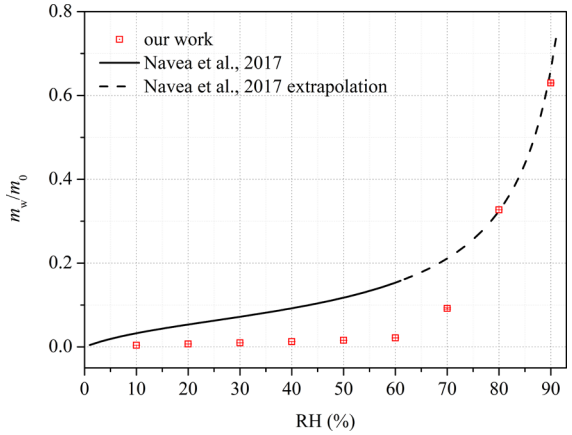


**Figure 3.** Comparison of mass ratios of adsorbed water to dry samples ($m_w/m_0$) for BCR-176R obtained by Navea et al.[36] and in our work.

$$\frac{m_w}{m_0} = A_F \bullet \sqrt[B_F]{RH} \quad (1)$$

where $m_w$ and $m_0$ are the mass of adsorbed water and dry samples, and $A_F$ and $B_F$ are empirical Freundlich parameters that are related to adsorption capacity and strength, respectively.

Table 2 summarizes $A_F$ and $B_F$ obtained in this work for all the 11 samples investigated. The values of $A_F$ varied by more than 4 orders of magnitude, ranging from <0.1% (GBW11129a and GBW11131a) to ~1.29 (BCR-176R), while the variation of $B_F$ was much smaller, ranging from ~0.12 (UPM1648a) to ~1.58 (CFA-2691). In addition, samples with higher $m_w/m_0$ at

**Table 2. Mass Ratio of Adsorbed Water to the Dry Sample ($m_w/m_0$) at 90% RH and $A_F$ and $B_F$ Derived Using the Freundlich Adsorption Isotherm Model for the 11 Samples Investigated**[a]

| sample | $m_w/m_0$ ($\times 10^{-3}$) | $A_F$ | $B_F$ |
|---|---|---|---|
| BCR-176R | 629.6 ± 1.9 | 1.29 ± 0.08 | 0.15 ± 0.01 |
| BCR-615 | 734.0 ± 3.0 | 1.09 ± 0.07 | 0.25 ± 0.02 |
| OFA | 272.1 ± 3.0 | 0.34 ± 0.02 | 0.39 ± 0.03 |
| UPM1648a | 183.5 ± 0.1 | 0.42 ± 0.07 | 0.12 ± 0.02 |
| CFA-2689 | 1.5 ± 0.1 | (1.50 ± 0.05) × $10^{-3}$ | 1.37 ± 0.10 |
| CFA-2690 | 1.2 ± 0.1 | (1.36 ± 0.02) × $10^{-3}$ | 1.21 ± 0.04 |
| CFA-2691 | 1.0 ± 0.1 | (0.99 ± 0.05) × $10^{-3}$ | 1.58 ± 0.18 |
| GBW08401 | 3.0 ± 0.1 | (3.12 ± 0.08) × $10^{-3}$ | 1.06 ± 0.06 |
| GBW11128a | 2.7 ± 0.1 | (2.76 ± 0.30) × $10^{-3}$ | 0.61 ± 0.11 |
| GBW11129a | 0.6 ± 0.1 | (0.55 ± 0.03) × $10^{-3}$ | 1.27 ± 0.14 |
| GBW11131a | 0.3 ± 0.1 | (0.35 ± 0.01) × $10^{-3}$ | 1.21 ± 0.10 |

[a]All the errors provided are standard deviations.

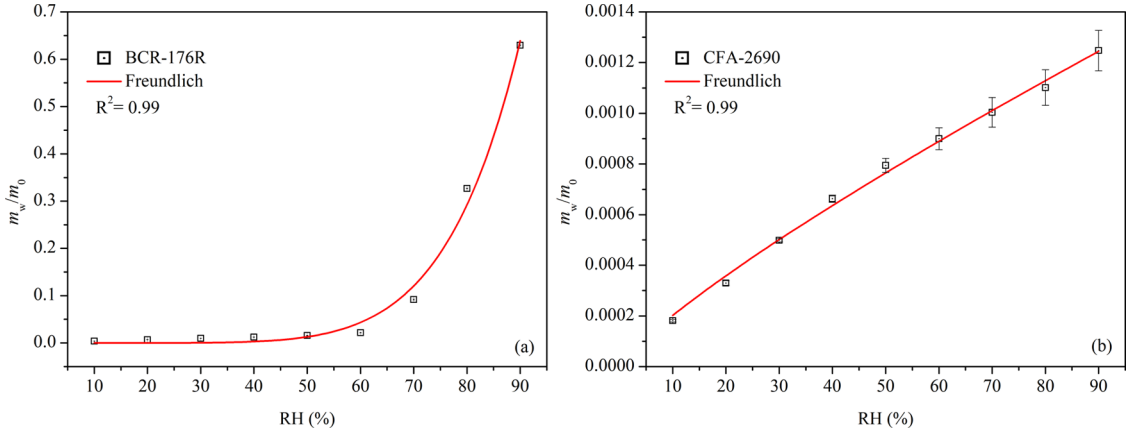


**Figure 4.** Mass ratios of adsorbed water to dry samples ($m_w/m_0$) as a function of RH (0–90%) at 25 °C for (a) BCR-176R and (b) CFA-2690. The experimental data were fitted with the Freundlich adsorption isotherm model (solid curves).


https://dx.doi.org/10.1021/acsearthspacechem.0c00219
ACS Earth Space Chem. 2020, 4, 1823−1830

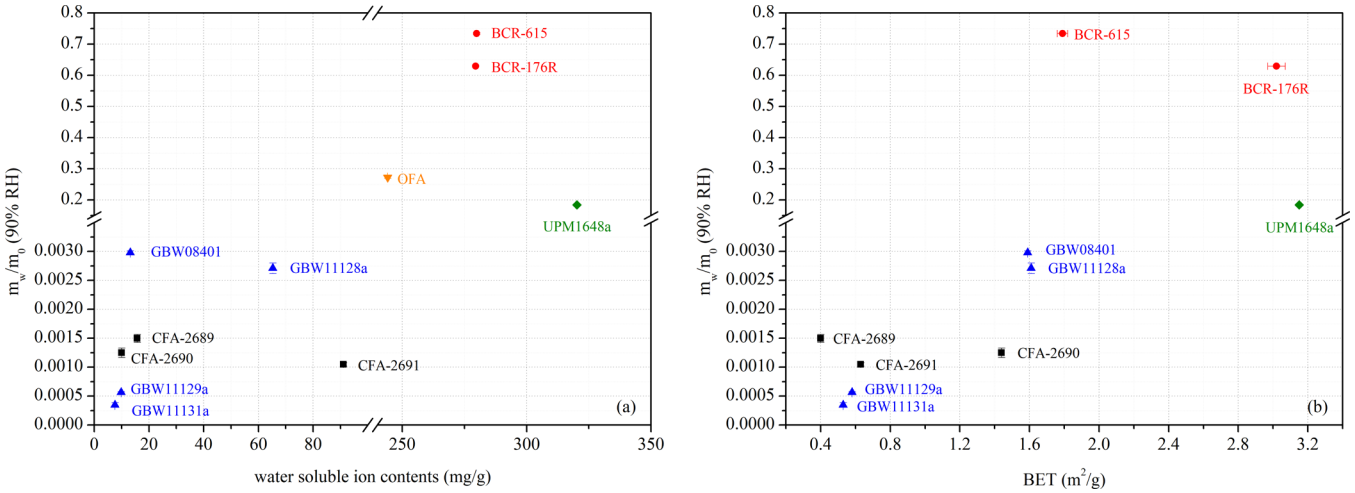


**Figure 5.** Dependence of mass ratios of adsorbed water to dry samples ($m_w/m_0$) at 90% RH on (a) water-soluble ion contents and (b) BET surface areas for the 11 unconventional mineral dust samples investigated in this study.

90% RH showed higher $A_F$ values, indicating stronger water adsorption capacity. For example, $A_F$ was determined to be 1.29 for BCR-176R ($m_w/m_0$ = 0.63 at 90% RH), ~3 orders of magnitude larger than that ($3.5 \times 10^{-4}$) for GBW11131a ($m_w/m_0$ = 0.0003 at 90% RH).

As mentioned above, two experimental techniques were employed to explore the water adsorption on unconventional mineral dust. Thus, we attempted to compare our DRIFTS results to the VSA results, although the integrated areas of IR spectra are only semiquantitative representations of the amounts of adsorbed water. As shown in Figure S4, good linear relationships ($R^2$ higher than 0.96) between integrated areas of IR peaks and $m_w/m_0$ were found for most samples; however, exceptions were also observed for BCR-615, CFA-2689, and CFA-2690 ($R^2$ in range of 0.74−0.85). In our previous study,[42] DRIFTS and VSA were also used to explore the hygroscopicity of pollen species, and good linear relationships were found between the two measurement techniques. To summarize, although good correlations between DRIFTS results and VSA results have been frequently observed, there are also exceptions. This is very likely because various factors, e.g., size of particles under investigation and how particles are packed in the sample cell, would impact the response of DRIFTS signals to the amount of adsorbed water.

Table 2 reveals that water uptake ability at 90% RH, represented by $m_w/m_0$, can be generally described by the following order: municipal waste fly ash > oil fly ash > road dust > coal fly ash: $m_w/m_0$ at 90% RH were ~0.63 and ~0.73 for BCR-176R and BCR-615, followed by OFA (~0.27) and UPM1648a (~0.18). Water uptake of coal fly ash was very limited, and their $m_w/m_0$ at 90% RH were all found to be <0.01; in other words, the mass increase of coal fly ash samples at 90% RH, relative to that at <1% RH, did not exceed 1%.

## DISCUSSIONS

The 11 unconventional mineral dust samples studied in this work came from different sources and showed different hygroscopic properties. The water adsorption and hygroscopicity of conventional mineral dust samples were summarized and discussed previously.[35,39] For example, Chen et al.[39] explored hygroscopic properties of 21 mineral dust samples, and their $m_w/m_0$ at 90% RH ranged from 0.0011 to 0.3080. Compared to conventional mineral dust, larger variations in hygroscopic properties were found in the present work for unconventional mineral dust. Moreover, water adsorption capacities of municipal waste fly ash were obviously larger than other mineral dust; however, this conclusion is rather tentative due to the very limited numbers of samples examined.

In addition to hygroscopic properties, we also measured water-soluble inorganic ion compositions for the 11 samples. Water-soluble ion contents were suggested as a key factor to affect water uptake properties of dust samples.[38,51] For example, Gaston et al.[51] used water-soluble ion contents as input in an aerosol thermodynamic model (ISORROPIA-II) to predict hygroscopicity of playa dust samples and found that the predicted single hygroscopicity parameter ($\kappa$) matched reasonably well with the measured $\kappa$ values for most of the samples examined. Figure 5a shows the dependence of $m_w/m_0$ at 90% RH on soluble ion contents for the 11 samples examined in our work, and it can be seen that samples with larger soluble ion contents in general exhibited larger capacities to adsorb water. For example, water-soluble ion contents were in the range of 8−91 mg/g for the seven coal fly ash samples investigated, much lower than the other four unconventional mineral dust samples (244−320 mg/g), and accordingly, their hygroscopicity, represented by $m_w/m_0$ at 90% RH, were significantly lower. However, a specific relationship is not apparent, indicating that other factors also affected their water uptake ability. In our recent study,[39] the water uptake capacities were found to fairly increase with BET surface area for mineral dust samples. Figure 5b shows the dependence of $m_w/m_0$ at 90% RH on BET surface area for the unconventional mineral dust samples examined in the present study. It appears that $m_w/m_0$ at 90% RH also increased with BET surface area. In addition, previous studies[39,49,52] suggested that particle size, surface functional groups, and mineralogy could also affect the hygroscopicity of mineral dust.

## CONCLUSIONS

Unconventional mineral dusts, e.g., coal fly ash, oil fly ash, and road dust, have been identified as an important contributor to atmospheric particulate matters. However, their hygroscopic properties are still poorly understood. In this work, we


https://dx.doi.org/10.1021/acsearthspacechem.0c00219
ACS Earth Space Chem. 2020, 4, 1823−1830

employed a vapor sorption analyzer (VSA) and an in situ diffusion reflectance infrared Fourier transform spectroscopy (DRIFTS) to investigate water uptake by 11 unconventional mineral dust samples, including two municipal waste fly ash, one oil fly ash, one road dust, and seven coal fly ash samples.

DRIFTS measurements showed that several IR peaks, which could be assigned to adsorbed water, appeared when RH was increased from >1%, and their intensities increased with increasing RH. Furthermore, large variations in hygroscopicity for different samples, and the mass ratios of adsorbed water to dry samples ($m_w/m_0$) at 90% RH, varied between 0.0003 (GBW11131a) and 0.7340 (BCR-615). For the 11 samples examined in our work, $m_w/m_0$ at 90% RH were found to be largest for the two municipal waste fly ash samples and smallest for the seven coal fly ash samples; compared to conventional mineral dust, hygroscopicity is similar for coal fly ash but higher for oil fly ash, municipal waste fly ash, and road dust. We further found that the Freundlich adsorption isotherm model could well approximate the amount of adsorbed water as a function of RH for the 11 unconventional mineral dust samples, and $A_F$ and $B_F$ values were derived to be in the range of $3.5 \times 10^{-4}$–1.29 and 0.12–1.58, respectively. In addition, $m_w/m_0$ at 90% RH appeared to be positively correlated with water-soluble ion contents and BET surface areas of these samples. Our results highlight that the hygroscopicity of unconventional mineral dust, being different from conventional mineral dust, shows large variations and should be taken into account when assessing their environmental and climatic effects.

## ■ ASSOCIATED CONTENT

### Supporting Information

The Supporting Information is available free of charge at https://pubs.acs.org/doi/10.1021/acsearthspacechem.0c00219.

Integrated areas of IR peaks assigned to adsorbed water as a function of RH (Table S1); mass ratios of adsorbed water to the dry sample as a function of RH (Table S2); in situ DRIFTS spectra as a function of RH (Figures S1 and S2); mass ratios of adsorbed water to dry samples as a function of RH (Figure S3); and integrated areas of IR peaks assigned to adsorbed water versus the mass ratios of adsorbed water to dry samples (Figure S4) (PDF)

## ■ AUTHOR INFORMATION


### Corresponding Author

**Mingjin Tang** − *State Key Laboratory of Organic Geochemistry, Guangdong Key Laboratory of Environmental Protection and Resources Utilization, and Guangdong-Hong Kong-Macao Joint Laboratory for Environmental Pollution and Control Guangzhou Institute of Geochemistry and Center for Excellence in Regional Atmospheric Environment, Institute of Urban Environment, Chinese Academy of Sciences, Guangzhou 510640, China; University of Chinese Academy of Sciences, Beijing 100049, China;* orcid.org/0000-0002-8756-8445; Email: mingjintang@gig.ac.cn

### Authors

**Chao Peng** − *State Key Laboratory of Organic Geochemistry, Guangdong Key Laboratory of Environmental Protection and Resources Utilization, and Guangdong-Hong Kong-Macao Joint Laboratory for Environmental Pollution and Control Guangzhou Institute of Geochemistry, Chinese Academy of Sciences, Guangzhou 510640, China*

**Wenjun Gu** − *State Key Laboratory of Organic Geochemistry, Guangdong Key Laboratory of Environmental Protection and Resources Utilization, and Guangdong-Hong Kong-Macao Joint Laboratory for Environmental Pollution and Control Guangzhou Institute of Geochemistry, Chinese Academy of Sciences, Guangzhou 510640, China; University of Chinese Academy of Sciences, Beijing 100049, China*

**Rui Li** − *State Key Laboratory of Organic Geochemistry, Guangdong Key Laboratory of Environmental Protection and Resources Utilization, and Guangdong-Hong Kong-Macao Joint Laboratory for Environmental Pollution and Control Guangzhou Institute of Geochemistry, Chinese Academy of Sciences, Guangzhou 510640, China; University of Chinese Academy of Sciences, Beijing 100049, China*

**Qinhao Lin** − *Guangdong Key Laboratory of Environmental Catalysis and Health Risk Control, Guangzhou Key Laboratory Environmental Catalysis and Pollution Control, School of Environmental Science and Engineering, Institute of Environmental Health and Pollution Control, Guangdong University of Technology, Guangzhou 510006, China*

**Qingxin Ma** − *State Key Joint Laboratory of Environment Simulation and Pollution Control, Research Center for Eco-Environmental Sciences, Chinese Academy of Sciences, Beijing 100085, China;* orcid.org/0000-0002-9668-7008

**Shiguo Jia** − *School of Atmospheric Sciences and Guangdong Province Key Laboratory for Climate Change and Natural Disaster Studies, Sun Yat-sen University, Guangzhou 510275, China*

**Padmaja Krishnan** − *Department of Civil & Environmental Engineering, National University of Singapore, 117576, Singapore*

**Xinming Wang** − *State Key Laboratory of Organic Geochemistry, Guangdong Key Laboratory of Environmental Protection and Resources Utilization, and Guangdong-Hong Kong-Macao Joint Laboratory for Environmental Pollution and Control Guangzhou Institute of Geochemistry and Center for Excellence in Regional Atmospheric Environment, Institute of Urban Environment, Chinese Academy of Sciences, Guangzhou 510640, China; University of Chinese Academy of Sciences, Beijing 100049, China;* orcid.org/0000-0002-1982-0928

Complete contact information is available at: https://pubs.acs.org/10.1021/acsearthspacechem.0c00219


### Author Contributions

◆C.P. and W.G. contributed equally to this work.

### Notes

The authors declare no competing financial interest.

## ■ ACKNOWLEDGMENTS

This work was supported by the National Natural Science Foundation of China (91744204), Guangdong Foundation for Program of Science and Technology Research (2017B030314057 and 2019B121205006), and Guangdong Science and Technology Department (2017GC010501). M.T. would like to thank the CAS Pioneer Hundred Talents Program for providing a starting grant.

## ■ REFERENCES

(1) Textor, C.; Schulz, M.; Guibert, S.; Kinne, S.; Balkanski, Y.; Bauer, S.; Berntsen, T.; Berglen, T.; Boucher, O.; Chin, M.; Dentener,

F.; Diehl, T.; Easter, R.; Feichter, H.; Fillmore, D.; Ghan, S.; Ginoux, P.; Gong, S.; Kristjansson, J. E.; Krol, M.; Lauer, A.; Lamarque, J. F.; Liu, X.; Montanaro, V.; Myhre, G.; Penner, J.; Pitari, G.; Reddy, S.; Seland, O.; Stier, P.; Takemura, T.; Tie, X. Analysis and quantification of the diversities of aerosol life cycles within AeroCom. *Atmos. Chem. Phys.* **2006**, *6*, 1777−1813.

(2) Huneeus, N.; Schulz, M.; Balkanski, Y.; Griesfeller, J.; Prospero, J.; Kinne, S.; Bauer, S.; Boucher, O.; Chin, M.; Dentener, F.; Diehl, T.; Easter, R.; Fillmore, D.; Ghan, S.; Ginoux, P.; Grini, A.; Horowitz, L.; Koch, D.; Krol, M. C.; Landing, W.; Liu, X.; Mahowald, N.; Miller, R.; Morcrette, J. J.; Myhre, G.; Penner, J.; Perlwitz, J.; Stier, P.; Takemura, T.; Zender, C. S. Global dust model intercomparison in AeroCom phase I. *Atmos. Chem. Phys.* **2011**, *11*, 7781−7816.

(3) Ginoux, P.; Prospero, J. M.; Gill, T. E.; Hsu, N. C.; Zhao, M. Global-scale attribution of anthropogenic and natural dust sources and their emission rates based on MODIS Deep Blue aerosol products. *Rev. Geophys.* **2012**, *50*, RG3005.

(4) Zhang, R.; Jing, J.; Tao, J.; Hsu, S. C.; Wang, G.; Cao, J.; Lee, C. S. L.; Zhu, L.; Chen, Z.; Zhao, Y.; Shen, Z. Chemical characterization and source apportionment of $PM_{2.5}$ in Beijing: seasonal perspective. *Atmos. Chem. Phys.* **2013**, *13*, 7053−7074.

(5) Janssens-Maenhout, G.; Crippa, M.; Guizzardi, D.; Dentener, F.; Muntean, M.; Pouliot, G.; Keating, T.; Zhang, Q.; Kurokawa, J.; Wankmueller, R.; van der Gon, H. D.; Kuenen, J. J. P.; Klimont, Z.; Frost, G.; Darras, S.; Koffi, B.; Li, M. HTAP_v2.2: a mosaic of regional and global emission grid maps for 2008 and 2010 to study hemispheric transport of air pollution. *Atmos. Chem. Phys.* **2015**, *15*, 11411−11432.

(6) Snider, G.; Weagle, C. L.; Murdymootoo, K. K.; Ring, A.; Ritchie, Y.; Stone, E.; Walsh, A.; Akoshile, C.; Nguyen Xuan, A.; Balasubramanian, R.; Brook, J.; Qonitan, F. D.; Dong, J.; Griffith, D.; He, K.; Holben, B. N.; Kahn, R.; Lagrosas, N.; Lestari, P.; Ma, Z.; Misra, A.; Norford, L. K.; Quel, E. J.; Salam, A.; Schichtel, B.; Segev, L.; Tripathi, S.; Wang, C.; Yu, C.; Zhang, Q.; Zhang, Y.; Brauer, M.; Cohen, A.; Gibson, M. D.; Liu, Y.; Martins, J. V.; Rudich, Y.; Martin, R. V. Variation in global chemical composition of $PM_{2.5}$: emerging results from SPARTAN. *Atmos. Chem. Phys.* **2016**, *16*, 9629−9653.

(7) Klimont, Z.; Kupiainen, K.; Heyes, C.; Purohit, P.; Cofala, J.; Rafaj, P.; Borken-Kleefeld, J.; Schoepp, W. Global anthropogenic emissions of particulate matter including black carbon. *Atmos. Chem. Phys.* **2017**, *17*, 8681−8723.

(8) Zheng, B.; Tong, D.; Li, M.; Liu, F.; Hong, C.; Geng, G.; Li, H.; Li, X.; Peng, L.; Qi, J.; Yan, L.; Zhang, Y.; Zhao, H.; Zheng, Y.; He, K.; Zhang, Q. Trends in China's anthropogenic emissions since 2010 as the consequence of clean air actions. *Atmos. Chem. Phys.* **2018**, *18*, 14095−14111.

(9) Chen, S.; Zhang, X.; Lin, J.; Huang, J.; Zhao, D.; Yuan, T.; Huang, K.; Luo, Y.; Jia, Z.; Zang, Z.; Qiu, Y. a.; Xie, L. Fugitive Road Dust $PM_{2.5}$ Emissions and Their Potential Health Impacts. *Environ. Sci. Technol.* **2019**, *53*, 8455−8465.

(10) Pan, X.; Chin, M.; Gautam, R.; Bian, H.; Kim, D.; Colarco, P. R.; Diehl, T. L.; Takemura, T.; Pozzoli, L.; Tsigaridis, K.; Bauer, S.; Bellouin, N. A multi-model evaluation of aerosols over South Asia: common problems and possible causes. *Atmos. Chem. Phys.* **2015**, *15*, 5903−5928.

(11) Zhang, L.; Liu, L.; Zhao, Y.; Gong, S.; Zhang, X.; Henze, D. K.; Capps, S. L.; Fu, T.-M.; Zhang, Q.; Wang, Y. Source attribution of particulate matter pollution over North China with the adjoint method. *Environ. Res. Lett.* **2015**, *10*, No. 084011.

(12) Philip, S.; Martin, R. V.; Snider, G.; Weagle, C. L.; van Donkelaar, A.; Brauer, M.; Henze, D. K.; Klimont, Z.; Venkataraman, C.; Guttikunda, S. K.; Zhang, Q. Anthropogenic fugitive, combustion and industrial dust is a significant, underrepresented fine particulate matter source in global atmospheric models. *Environ. Res. Lett.* **2017**, *12*, No. 044018.

(13) Weagle, C. L.; Snider, G.; Li, C.; van Donkelaar, A.; Philip, S.; Bissonnette, P.; Burke, I.; Jackson, J.; Latimer, R.; Stone, E.; Abboud, I.; Akoshile, C.; Nguyen Xuan, A.; Brook, J. R.; Cohen, A.; Dong, J.; Gibson, M. D.; Griffith, D.; He, K. B.; Holben, B. N.; Kahn, R.; Keller, C. A.; Kim, J. S.; Lagrosas, N.; Lestari, P.; Khian, Y. L.; Liu, Y.; Marais, E. A.; Martins, J. V.; Misra, A.; Muliane, U.; Pratiwi, R.; Quel, E. J.; Salam, A.; Segey, L.; Tripathi, S. N.; Wang, C.; Zhang, Q.; Brauer, M.; Rudich, Y.; Martin, R. V. Global Sources of Fine Particulate Matter: Interpretation of $PM_{2.5}$ Chemical Composition Observed by SPARTAN using a Global Chemical Transport Model. *Environ. Sci. Technol.* **2018**, *52*, 11670−11681.

(14) Jeong, J. I.; Park, R. J. Influence of the Anthropogenic Fugitive, Combustion, and Industrial Dust on Winter Air Quality in East Asia. *Atmosphere* **2019**, *10*, 790.

(15) Ojha, K.; Pradhan, N. C.; Samanta, A. N. Zeolite from fly ash: synthesis and characterization. *B. Mater. Sci.* **2004**, *27*, 555−564.

(16) Ramanathan, V.; Crutzen, P. J.; Kiehl, J. T.; Rosenfeld, D. Atmosphere - Aerosols, climate and the hydrological cycle. *Science* **2001**, *294*, 2119−2124.

(17) Chen, H.; Laskin, A.; Baltrusaitis, J.; Gorski, C. A.; Scherer, M. M.; Grassian, V. H. Coal Fly Ash as a Source of Iron in Atmospheric Dust. *Environ. Sci. Technol.* **2012**, *46*, 2112−2120.

(18) Li, W.; Xu, L.; Liu, X.; Zhang, J.; Lin, Y.; Yao, X.; Gao, H.; Zhang, D.; Chen, J.; Wang, W. Air pollution−aerosol interactions produce more bioavailable iron for ocean ecosystems. *Sci. Adv.* **2017**, *3*, No. e1601749.

(19) Grawe, S.; Augustin-Bauditz, S.; Clemen, H.-C.; Ebert, M.; Hammer, S. E.; Lubitz, J.; Reicher, N.; Rudich, Y.; Schneider, J.; Staacke, R.; Stratmann, F.; Welti, A.; Wex, H. Coal fly ash: linking immersion freezing behavior and physicochemical particle properties. *Atmos. Chem. Phys.* **2018**, *18*, 13903−13923.

(20) Kanakidou, M.; Myriokefalitakis, S.; Tsigaridis, K. Aerosols in atmospheric chemistry and biogeochemical cycles of nutrients. *Environ. Res. Lett.* **2018**, *13*, No. 063004.

(21) Umo, N. S.; Wagner, R.; Ullrich, R.; Kiselev, A.; Saathoff, H.; Weidler, P. G.; Cziczo, D. J.; Leisner, T.; Möhler, O. Enhanced ice nucleation activity of coal fly ash aerosol particles initiated by ice-filled pores. *Atmos. Chem. Phys.* **2019**, *19*, 8783−8800.

(22) Kim, D.; Xiao, Y.; Karchere-Sun, R.; Richmond, E.; Ricker, H. M.; Leonardi, A.; Navea, J. G. Atmospheric Processing of Anthropogenic Combustion Particles: Effects of Acid Media and Solar Flux on the Iron Mobility from Fly Ash. *ACS Earth Space Chem.* **2020**, *4*, 750−761.

(23) Harris, E.; Sinha, B.; van Pinxteren, D.; Tilgner, A.; Fomba, K. W.; Schneider, J.; Roth, A.; Gnauk, T.; Fahlbusch, B.; Mertes, S.; Lee, T.; Collett, J.; Foley, S.; Borrmann, S.; Hoppe, P.; Herrmann, H. Enhanced Role of Transition Metal Ion Catalysis During In-Cloud Oxidation of $SO_2$. *Science* **2013**, *340*, 727−730.

(24) Gankanda, A.; Coddens, E. M.; Zhang, Y. P.; Cwiertny, D. M.; Grassian, V. H. Sulfate formation catalyzed by coal fly ash, mineral dust and iron(III) oxide: variable influence of temperature and light. *Environ. Sci.: Processes Impacts* **2016**, *18*, 1484−1491.

(25) Schroth, A. W.; Crusius, J.; Sholkovitz, E. R.; Bostick, B. C. Iron solubility driven by speciation in dust sources to the ocean. *Nat. Geosci.* **2009**, *2*, 337−340.

(26) Ito, A. Atmospheric Processing of Combustion Aerosols as a Source of Bioavailable Iron. *Environ. Sci. Technol. Lett.* **2015**, *2*, 70−75.

(27) Wang, R.; Balkanski, Y.; Boucher, O.; Bopp, L.; Chappell, A.; Ciais, P.; Hauglustaine, D.; Penuelas, J.; Tao, S. Sources, transport and deposition of iron in the global atmosphere. *Atmos. Chem. Phys.* **2015**, *15*, 6247−7705.

(28) Parungo, F.; Ackerman, E.; Proulx, H.; Pueschel, R. Nucleation properties of fly-ash in a coal-fired power-plant plume. *Atmos. Environ.* **1978**, *12*, 929−935.

(29) Umo, N. S.; Murray, B. J.; Baeza-Romero, M. T.; Jones, J. M.; Lea-Langton, A. R.; Malkin, T. L.; O'Sullivan, D.; Neve, L.; Plane, J. M. C.; Williams, A. Ice nucleation by combustion ash particles at conditions relevant to mixed-phase clouds. *Atmos. Chem. Phys.* **2015**, *15*, 5195−5210.

(30) Grawe, S.; Augustin-Bauditz, S.; Hartmann, S.; Hellner, L.; Pettersson, J. B. C.; Prager, A.; Stratmann, F.; Wex, H. The immersion


https://dx.doi.org/10.1021/acsearthspacechem.0c00219
ACS Earth Space Chem. 2020, 4, 1823−1830

freezing behavior of ash particles from wood and brown coal burning. *Atmos. Chem. Phys.* **2016**, *16*, 13911−13928.
(31) Losey, D. J.; Sihvonen, S. K.; Veghte, D. P.; Chong, E.; Freedman, M. A. Acidic processing of fly ash: chemical characterization, morphology, and immersion freezing. *Environ. Sci.: Processes Impacts* **2018**, *20*, 1581−1592.
(32) Borcherding, J. A.; Chen, H. H.; Caraballo, J. C.; Baltrusaitis, J.; Pezzulo, A. A.; Zabner, J.; Grassian, V. H.; Comellas, A. P. Coal Fly Ash Impairs Airway Antimicrobial Peptides and Increases Bacterial Growth. *PLoS One* **2013**, *8*, No. e57673.
(33) Buonfiglio, L. G. V.; Mudunkotuwa, I. A.; Abou Alaiwa, M. H.; Calderon, O. G. V.; Borcherding, J. A.; Gerke, A. K.; Zabner, J.; Grassian, V. H.; Comellas, A. P. Effects of Coal Fly Ash Particulate Matter on the Antimicrobial Activity of Airway Surface Liquid. *Environ. Health Persp.* **2017**, *125*, No. 077003.
(34) Tang, M.; Chan, C. K.; Li, Y. J.; Su, H.; Ma, Q.; Wu, Z.; Zhang, G.; Wang, Z.; Ge, M.; Hu, M.; He, H.; Wang, X. A review of experimental techniques for aerosol hygroscopicity studies. *Atmos. Chem. Phys.* **2019**, *19*, 12631−12686.
(35) Tang, M.; Cziczo, D. J.; Grassian, V. H. Interactions of Water with Mineral Dust Aerosol: Water Adsorption, Hygroscopicity, Cloud Condensation, and Ice Nucleation. *Chem. Rev.* **2016**, *116*, 4205−4259.
(36) Navea, J. G.; Richmond, E.; Stortini, T.; Greenspan, J. Water Adsorption Isotherms on Fly Ash from Several Sources. *Langmuir* **2017**, *33*, 10161−10171.
(37) Fu, H.; Lin, J.; Shang, G.; Dong, W.; Grassian, V. H.; Carmichael, G. R.; Li, Y.; Chen, J. Solubility of Iron from Combustion Source Particles in Acidic Media Linked to Iron Speciation. *Environ. Sci. Technol.* **2012**, *46*, 11119−11127.
(38) Tang, M.; Zhang, H.; Gu, W.; Gao, J.; Jian, X.; Shi, G.; Zhu, B.; Xie, L.; Guo, L.; Gao, X. Hygroscopic properties of saline mineral dust from different regions in China: geographical variations, compositional dependence and atmospheric implications. *J. Geophys. Res.-Atmos.* **2019**, *124*, 10844−10857.
(39) Chen, L.; Peng, C.; Nenes, A.; Gu, W.; Fu, H.; Jian, X.; Zhang, H.; Zhang, G.; Zhu, J.; Wang, X.; Tang, M. On mineral dust aerosol hygroscopicity. *Atmos. Chem. Phys. Discuss.* **2020**, *2020*, 1−37.
(40) Li, R.; Jia, X.; Wang, F.; Ren, Y.; Wang, X.; Zhang, H.; Li, G.; Wang, X.; Tang, M. Heterogeneous reaction of $NO_2$ with hematite, goethite and magnetite: Implications for nitrate formation and iron solubility enhancement. *Chemosphere* **2020**, *242*, 125273−125273.
(41) Ma, Q.; He, H.; Liu, Y. In situ DRIFTS study of hygroscopic behavior of mineral aerosol. *J. Environ. Sci.* **2010**, *22*, 555−560.
(42) Tang, M.; Gu, W.; Ma, Q.; Li, Y. J.; Zhong, C.; Li, S.; Yin, X.; Huang, R.-J.; He, H.; Wang, X. Water adsorption and hygroscopic growth of six anemophilous pollen species: the effect of temperature. *Atmos. Chem. Phys.* **2019**, *19*, 2247−2258.
(43) Gu, W.; Li, Y.; Zhu, J.; Jia, X.; Lin, Q.; Zhang, G.; Ding, X.; Song, W.; Bi, X.; Wang, X.; Tang, M. Investigation of water adsorption and hygroscopicity of atmospherically relevant particles using a commercial vapor sorption analyzer. *Atmos. Meas. Tech.* **2017**, *10*, 3821−3832.
(44) Chen, L.; Chen, Y.; Chen, L.; Gu, W.; Peng, C.; Luo, S.; Song, W.; Wang, Z.; Tang, M. Hygroscopic Properties of 11 Pollen Species in China. *ACS Earth Space Chem.* **2019**, *3*, 2678−2683.
(45) Guo, L.; Gu, W.; Peng, C.; Wang, W.; Li, Y. J.; Zong, T.; Tang, Y.; Wu, Z.; Lin, Q.; Ge, M.; Zhang, G.; Hu, M.; Bi, X.; Wang, X.; Tang, M. A comprehensive study of hygroscopic properties of calcium- and magnesium-containing salts: implication for hygroscopicity of mineral dust and sea salt aerosols. *Atmos. Chem. Phys.* **2019**, *19*, 2115−2133.
(46) Goodman, A. L.; Bernard, E. T.; Grassian, V. H. Spectroscopic study of nitric acid and water adsorption on oxide particles: Enhanced nitric acid uptake kinetics in the presence of adsorbed water. *J. Phys. Chem. A* **2001**, *105*, 6443−6457.
(47) Al-Abadleh, H. A.; Grassian, V. H. FT-IR study of water adsorption on aluminum oxide surfaces. *Langmuir* **2003**, *19*, 341−347.
(48) Joshi, N.; Romanias, M. N.; Riffault, V.; Thevenet, F. Investigating water adsorption onto natural mineral dust particles: Linking DRIFTS experiments and BET theory. *Aeolian Res.* **2017**, *27*, 35−45.
(49) Ibrahim, S.; Romanias, M. N.; Alleman, L. Y.; Zeineddine, M. N.; Angeli, G. K.; Trikalitis, P. N.; Thevenet, F. Water Interaction with Mineral Dust Aerosol: Particle Size and Hygroscopic Properties of Dust. *ACS Earth Space Chem.* **2018**, *2*, 376−386.
(50) Hatch, C. D.; Wiese, J. S.; Crane, C. C.; Harris, K. J.; Kloss, H. G.; Baltrusaitis, J. Water Adsorption on Clay Minerals As a Function of Relative Humidity: Application of BET and Freundlich Adsorption Models. *Langmuir* **2012**, *28*, 1790−1803.
(51) Gaston, C. J.; Pratt, K. A.; Suski, K. J.; May, N. W.; Gill, T. E.; Prather, K. A. Laboratory Studies of the Cloud Droplet Activation Properties and Corresponding Chemistry of Saline Playa Dust. *Environ. Sci. Technol.* **2017**, *51*, 1348−1356.
(52) Yesilbas, M.; Boily, J.-F. Particle Size Controls on Water Adsorption and Condensation Regimes at Mineral Surfaces. *Sci. Rep.* **2016**, *6*, 32136.


https://dx.doi.org/10.1021/acsearthspacechem.0c00219
*ACS Earth Space Chem.* 2020, 4, 1823−1830